Science of the Total Environment 663 (2019) 644–653

Contents lists available at ScienceDirect

Science of the Total Environment

journal homepage: www.elsevier.com/locate/scitotenv

Global exposure to rainstorms and the contribution rates of climate change and population change

Xinli Liao [a,b], Wei Xu [a,b,*], Junlin Zhang [a,b], Ying Li [a,b], Yugang Tian [c]

[a] Key Laboratory of Environmental Change and Natural Disaster of Ministry of Education, Faculty of Geographical Science, Beijing Normal University, Beijing 100875, China
[b] Academy of Disaster Reduction and Emergency Management, Ministry of Emergency Management and Ministry of Education, Beijing Normal University, Beijing 100875, China
[c] Faculty of Information Engineering, China University of Geosciences, Wuhan 430074, China

HIGHLIGHTS

- Global population exposure to rainstorms and contribution rates are analyzed.
- Population exposure shows a linear upward trend in most regions.
- Change in total global exposure is mainly due to the population change effect.

GRAPHICAL ABSTRACT

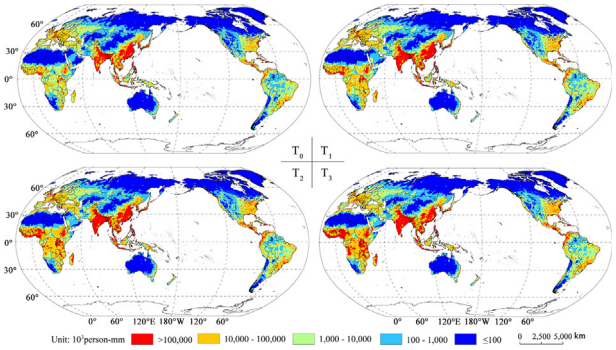

ARTICLE INFO

Article history:
Received 15 October 2018
Received in revised form 22 January 2019
Accepted 22 January 2019
Available online 25 January 2019

Editor: SCOTT SHERIDAN

Keywords:
Global climate change
Rainstorm
Population exposure
Contribution rate
Global scale

ABSTRACT

Quantifying global population exposure to rainstorms is a key component of population risk assessments for rainstorms and induced floods. Based on daily precipitation data from the NEX-GDDP dataset, rainfall from rainstorms is first calculated by a multi-model ensemble method for four periods from 1986 to 2100. Combined with population data from the SSP2 scenario, the global population exposure to rainstorms is then calculated and analyzed. Finally, the contribution rates of climate change effect, population change effect, and joint change effect on exposure change are quantitatively assessed. The results showed that (1) Population exposure to rainstorms shows a linear upward trend from base period to the late 21st century period in most regions, and the mid-21st century period compared with base period has the fastest rate of increase. (2) The spatial patterns of population exposure to rainstorms are very similar for the four periods and the areas with high exposure are mainly distributed in Asia, population exposure of Africa is gradually increasing. The countries with high exposure show little volatility, especially the top eight countries. (3) The change in total exposure is mainly due to population change. Based on the composition of the total exposure change for each country, the number of countries whose climate change effect is greater than that of population change is gradually increasing, and this number reaches more than a quarter of the total when the late 21st century period is compared with the mid-21st century period.

1. Introduction

There has been an increasing trend in the frequency and intensity of extreme weather/climate events due to global warming (Alexander et al., 2006; Min et al., 2011; Westra et al., 2013). With global warming, there are likely more land regions where the number of heavy

* Corresponding author at: Key Laboratory of Environmental Change and Natural Disaster of Ministry of Education, Faculty of Geographical Science, Beijing Normal University, Beijing 100875, China.
E-mail address: xuwei@bnu.edu.cn (W. Xu).

https://doi.org/10.1016/j.scitotenv.2019.01.290
0048-9697/

precipitation events has increased than where it has decreased (IPCC, 2014). Extreme daily precipitation averaged over both dry and wet climatic regimes showed robust increases in both observations and climate models from 1951 to 2010 (Donat et al., 2016). A significant intensification of daily precipitation extremes for all seasons is projected for the middle and high latitudes of both hemispheres at the end of the present century (Toreti et al., 2013). Recent detection of increasing trends in extreme precipitation and discharge in some catchments implies greater risks of flooding (medium confidence) at regional scale (IPCC, 2014). Changes in extreme precipitation and its induced destructive floods are among the most relevant consequences of climate warming and have been attracting wide attentions. And, with the socioeconomic development, the population, assets and other exposures exposed to natural hazards are increasing (Hanson et al., 2011; Jongman et al., 2015; Jongman et al., 2012; Winsemius et al., 2018). Especially the urbanization, aging and accumulative wealth will amplify the exposure (Qin et al., 2015; Popp et al., 2017). In addition, the global urban land that lies within the low elevation coastal zone will increase 230% from 2000 to 2030 (Güneralp et al., 2015), which also will increase the population exposed to rainstorms. Risk management and adaptation to climate change mainly focus on reducing exposure and vulnerability and increasing resilience to the potential adverse impacts of climate extremes (IPCC, 2012). Therefore, exploring the exposure is necessary for disaster loss and risk assessments. The population exposure to extreme precipitation events would increase depending on the degree of warming, and the 0.5 °C less warming would reduce exposure to once-in-20-year extreme precipitation events by 36% in global land monsoon regions (Zhang et al., 2018). The elderly population in rainstorm hazard areas in China increased by 110 million with a rate of 14.6% from 1990 to 2010 (Liang et al., 2017). While there have been many studies on population exposures, particularly for floods, obtaining detailed information on exposure to rainstorms at the global scale remains an open challenge currently. Also, there is little done about the contribution rates to the exposure change.

In this study, the global population exposure to rainstorms for four periods from 1986 to 2100 was first calculated based on daily precipitation data from the National Aeronautics and Space Administration (NASA) Earth Exchange Global Daily Downscaled Projections (NEX-GDDP) dataset and population data from the Shared Socioeconomic Pathways (SSPs) provided by the Inter-Sectoral Impact Model Intercomparison Project (ISIMIP). Then, the spatiotemporal patterns of exposure are discussed at the global, continental, and country levels. Finally, the contribution rates of the climate change effect, population change effect, and joint change effect on exposure change are quantitatively assessed. Based on this analysis of exposure and the relative contributions of different contributors, we aimed to characterize the future changes in rainstorm-related population exposure and clarify the importance of climate change and population change to this exposure change.

2. Data and research methods

2.1. Data sources

Precipitation data and population data were used in this study. We used the NEX-GDDP dataset, which was released by NASA in June 2015, to estimate the future climate changes, and the data can be downloaded from the NASA website (https://dataserver.nccs.nasa.gov/thredds/catalog/bypass/NEX-GDDP/catalog.html). This dataset was obtained by using the Bias-Correction Spatial Disaggregation (BCSD) method for the general circulation model (GCM) runs conducted under the Coupled Model Intercomparison Project Phase 5 (CMIP5) (Wood et al., 2002; Wood et al., 2004; Maurer and Hidalgo, 2008; Thrasher et al., 2012), so it has higher spatial resolution and accuracy. Some studies show that NEX-GDDP improves the significant underestimation of rainfall extremes found in CMIP5 (Chen et al., 2017; Sahany et al., 2018). The temporal and spatial resolutions of the dataset are 1 day and 0.25° × 0.25°, respectively. The dataset compiles 42 climate projections from 21 CMIP5 GCMs (Supplementary Table S1) and two of the four greenhouse gas emissions scenarios, known as Representative Concentration Pathways (RCP 4.5 and RCP 8.5) for the period from 2006 to 2100 (2 of the 21 models only provide data through 2099), as well as the historical experiment for each model for the period from 1950 to 2005. The RCP4.5 scenario, which is an intermediate stabilization pathway and is more consistent with the current emission reduction measures and effects, is selected for this study.

To estimate the future changes in population, we used the projections from the Shared Socioeconomic Pathways (SSPs). It contains five emission scenarios, known as SSP1–5. These data provided by the Inter-Sectoral Impact Model Intercomparison Project (ISIMIP) can be downloaded from the ISIMIP website (http://clima-dods.ictp.it/Users/fcolon_g/ISI-MIP/). The SSP2 scenario represents intermediate challenges to both mitigation and adaptation (O'Neill et al., 2017; Van Vuuren and Carter, 2013), is mostly consistent with the RCP4.5. Hence, the population under the SSP2 scenario was selected for this study. The temporal and spatial resolutions of the dataset are 1 year and 0.5° × 0.5°, respectively.

To facilitate a comparative and statistical analysis, according to the Intergovernmental Panel on Climate Change (IPCC) Fifth Assessment Report (IPCC, 2014), we selected the period from 1986 to 2005 as the base period (T_0), 2016–2035 as the early 21st century period (T_1), 2046–2065 as the mid-21st century period (T_2), and 2081–2100 as the late 21st century period (T_3). T_{1-0} represents T_1 compared with T_0, T_{2-1}, T_{3-2}, and T_{3-0} follow the same rule. To maintain spatial consistency, precipitation data were resampled to 0.5° × 0.5° grids by the bilinear interpolation method.

2.2. Methods

2.2.1. Rainstorm intensity and population

To our best knowledge, it is more reasonable to use absolute threshold for the small scale region, and it is more reasonable to use relative threshold for the large scale region. So in this study, rainstorm was defined by daily precipitation exceeding a given threshold, which was in turn defined as the 95th percentile value for each 0.5° × 0.5° grid. The method improved by Bonsal et al. (2001) was used when calculating the threshold, in which daily precipitation data for each year were first ranked in ascending order $X_1, X_2, \ldots, X_N$, and the probability P_{ro} that a random value is less than or equal to the rank of that value X_m was estimated by Eq. (1).

$$P_{ro} = (m-0.31)/(N+0.38) \quad (1)$$

where m is the rank, and N is the number of samples. For example, if there are 90 values, the 95th percentile value is linearly interpolated between the 87th-ranked value (corresponding to $P_{ro} = 95.9\%$) and the 86th-ranked value ($P_{ro} = 94.8\%$).

We first calculated the threshold of each model for each year, then calculated the average of 20 years' in each period, which represents the threshold of each model for each period. Multi-model ensemble (MME) are widely used in research especially for global-scale climate change studies because it is generally found to have a better performance than single models (Barfus and Bernhofer, 2014; Palmer et al., 2005; Samouly et al., 2018). So in this study, the average of the individual rainstorm thresholds of the 21 models was calculated and used as the rainstorm threshold for each grid. Based on the threshold value, we calculated the annual rainfall from rainstorms by accumulating daily precipitation exceeding the threshold in a certain year for each model, then used the 20-year averages of the rainfall in each period to represent the rainstorm intensity, and rainfall from rainstorms was the average of 21 models too. The reason that we used 20-year averages is to minimize inter-annual variations. The global, continental, and country scale rainfall from rainstorms is the sum of that in all grids covered by each polygon, population and exposure use the sum too.

Since the temporal resolution of the population data is 1 year, population is the average of 20 years in each period.

2.2.2. Population exposure to rainstorms

According to the United Nations International Strategy for Disaster Reduction (UNISDR, 2017), population exposure to rainstorms is defined as the population in rainstorm-prone areas. The exposure can be computed by multiplying the rainstorm intensity and population for each grid. Therefore, the spatial resolution of population exposure is 0.5°×0.5°, and the measurement unit of population exposure to rainstorms is person-mm.

2.2.3. Change rate of the total rainfall from rainstorms, population, and exposure

This study used change rate, which is a relative value, to analyze the magnitude of change for rainfall from rainstorms, population, and exposure.

$$C\_Rate = (C_j - C_i)/C_i \times 100\% \quad (2)$$

$$P\_Rate = (P_j - P_i)/P_i \times 100\% \quad (3)$$

$$E\_Rate = (E_j - E_i)/E_i \times 100\% \quad (4)$$

where *C_Rate* represents the rainfall from rainstorms' change rate, *P_Rate* represents the population's change rate, *E_Rate* represents the exposure's change rate. C_i and C_j represent the rainfall from rainstorms in period *i* and *j*, respectively. P_i and P_j represent the population in period *i* and *j*, respectively. E_i and E_j represent the exposure in period *i* and *j*, respectively.

2.2.4. Rate of contribution to the total exposure change

According to Jones et al. (2015) and Liu et al. (2017), the influence on exposure change can be divided into three parts: the climate change effect (measured by allowing climate to change with time but keeping the population fixed at a reference period level), the population change effect (measured by allowing population change but keeping the climate fixed at a reference period level), and the joint change effect (measured by the total exposure change minus the summation of the climate and population change effect related changes). The decomposition for exposure change is calculated according to Eq. (5).

$$\Delta E = P_j \times C_j - P_i \times C_i = P_i \times \Delta C + \Delta P \times C_i + \Delta P \times \Delta C \quad (5)$$

where ΔE represents the total change in exposure. P_i and C_i represent the population and rainfall from rainstorms in period *i*, respectively. P_j and C_j represent the population and rainfall from rainstorms in period *j*, respectively. ΔP and ΔC represent the changes in population and rainfall from rainstorms from period *i* to period *j*, respectively. $P_i \times \Delta C$ represents the climate change effect, $C_i \times \Delta P$ represents the population change effect, and $\Delta C \times \Delta P$ represents the joint change effect.

Therefore, the contribution rate of each factor is calculated according to:

$$CR_{cli} = \frac{|P_i \times \Delta C|}{|P_i \times \Delta C| + |\Delta P \times C_i| + |\Delta P \times \Delta C|} \times 100\% \quad (6)$$

$$CR_{pop} = \frac{|C_i \times \Delta P|}{|P_i \times \Delta C| + |\Delta P \times C_i| + |\Delta P \times \Delta C|} \times 100\% \quad (7)$$

$$CR_{cli-pop} = \frac{|\Delta P \times \Delta C|}{|P_i \times \Delta C| + |\Delta P \times C_i| + |\Delta P \times \Delta C|} \times 100\% \quad (8)$$

where CR_{cli} represents the contribution rate of the climate change effect, CR_{pop} represents the contribution rate of the population change effect, and $CR_{cli\text{-}pop}$ represents the contribution rate of the joint change effect.

3. Results

3.1. Changes in rainstorms and population

Fig. 1 shows that the spatial patterns of MME's rainfall from rainstorms for the four periods are very similar, and regions with high rainfall from rainstorms are mainly distributed in the coastal areas of Asia (e.g., India, Japan, the Philippines, Indonesia, and Myanmar) and northern South America (e.g., Columbia and Ecuador). The total global rainfall

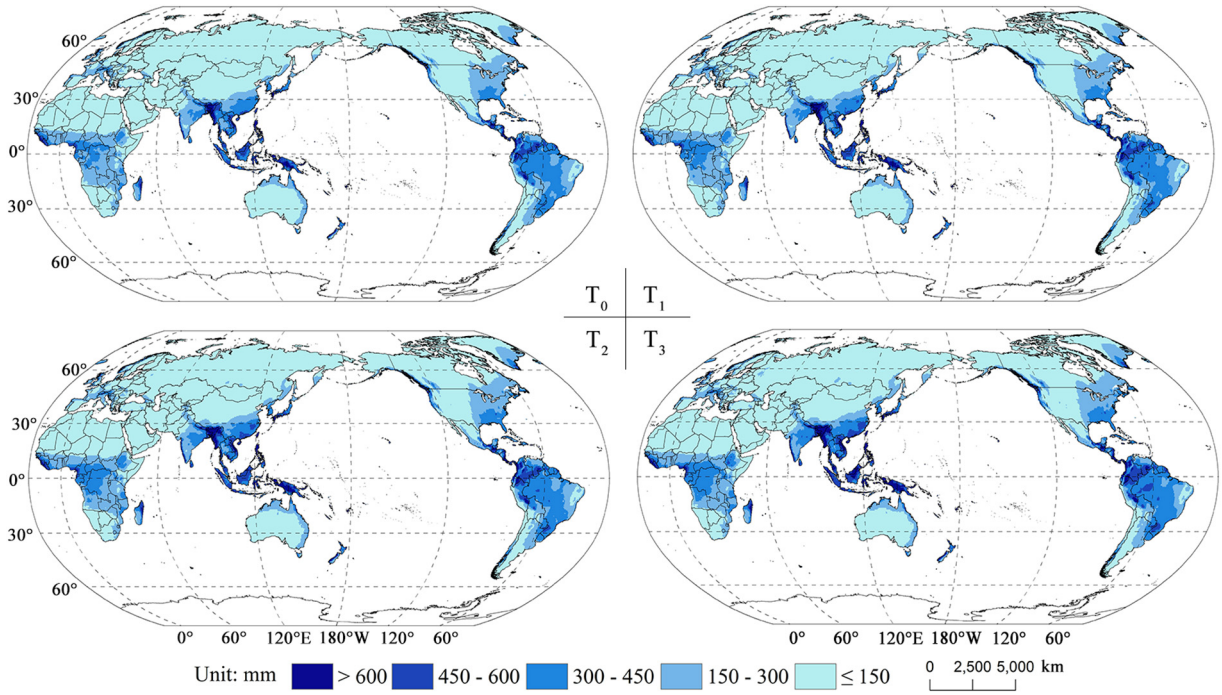

Fig. 1. Spatial distribution of the global rainfall from rainstorms.

Table 1
Total rainfall from rainstorms and the change rates.

	Total rainfall from rainstorms (10^6 mm)				*C_Rate* (%)			
	T_0	T_1	T_2	T_3	T_{1-0}	T_{2-1}	T_{3-2}	T_{3-0}
Global	8.48	8.87	9.23	9.89	5	4	7	17
*Asia	2.58	2.76	2.92	3.17	7	6	9	23
*North America	1.70	1.80	1.89	2.02	6	5	7	19
*Europe	0.72	0.75	0.78	0.84	4	3	7	16
*Africa	1.39	1.44	1.49	1.59	4	3	7	14
*South America	1.71	1.75	1.77	1.88	2	1	6	10
*Oceania	0.37	0.37	0.38	0.39	1	3	1	6

Table 2
Total population and the change rates.

	Total population (10^9 person)				*P_Rate* (%)			
	T_0	T_1	T_2	T_3	T_{1-0}	T_{2-1}	T_{3-2}	T_{3-0}
Global	5.42	7.59	8.96	9.37	40	18	5	73
*Asia	3.34	4.53	4.87	4.31	36	7	−11	29
*North America	0.43	0.58	0.68	0.73	36	18	7	71
*Europe	0.64	0.66	0.62	0.56	2	−5	−10	−12
*Africa	0.70	1.37	2.28	3.28	96	66	44	369
*South America	0.30	0.42	0.48	0.46	41	14	−4	54
*Oceania	0.02	0.03	0.04	0.04	44	16	2	70

from rainstorms shows a linear upward trend, with a change rate of 17% from T_0 to T_3. The areas with high rainfall from rainstorms gradually expand from T_0 to T_3. At the continental scale, Asia has the largest total rainfall from rainstorms for each period, and it also has the largest change rate of 23% from T_0 to T_3, while Oceania has the smallest total rainfall from rainstorms and change rate of 6% (Table 1).

The spatial patterns of the population for the four periods are also very similar, and regions with large populations are mainly distributed in Asia (e.g., China, India, and Japan) (Fig. 2). From T_0 to T_3, the total global population shows an increasing trend, with a change rate of 73%. Total population change for North America, Africa, and Oceania shows the same trend as that globally. Asia, Europe, and South America show a trend of increasing first and then decreasing. For T_{3-0} Africa has the largest change rate of 369%, while this rate decreases by 12% over Europe (Table 2).

3.2. Spatial and temporal changes in the global, continental, and, country scale population exposure to rainstorms

Overall, the spatial distribution patterns of the global population exposure are similar for the four periods, and the areas with extremely high exposure (10^8 person-mm or more) and high exposure (10^7–10^8 person-mm) gradually increase from T_0 to T_3. In terms of spatial distribution, the areas with extremely high exposure are mainly distributed in East Asia (e.g., southeastern China, Korea, and Japan), South Asia (e.g., India and Bangladesh), Southeast Asia (e.g., the Philippines and Indonesia), and scattered distributions in Africa (e.g., Nigeria and Ethiopia). The areas with high exposure are scattered but mainly in Central Europe (e.g., Poland, Germany, and Czech Republic), Western Europe (e.g., Ireland and France), Central Africa (e.g., Congo (Kinshasa)), Southern Africa (e.g., Zambia), and the eastern United States. The areas with medium exposure (10^6–10^7 person-mm) are mainly distributed in Eastern Europe (e.g., Ukraine, Belarus, and the European part of Russia) and northwestern Brazil. The areas with low exposure (10^5–10^6 person-mm) are mainly distributed in Asia (e.g., Saudi Arabia, Kazakhstan, and the northwest of China), the western United States, and scattered distributions in South America. The areas of extremely low exposure (10^5 person-mm and below) are widely distributed, mostly in high-latitude areas (e.g., Denmark, Russia, and Canada), Oceania, and North Africa (e.g., Sahara Desert). In more details, the spatial patterns in China and Africa have changed the most. The areas of China with extremely high exposure are getting smaller, while that of Africa is getting bigger (Fig. 3).

Temporally, the total global exposure shows a rapid increase from T_0 to T_1 and a slight increase from T_1 to T_3. The total exposure increases by 48% from T_0 to T_1, 22% from T_1 to T_2, and 11% from T_2 to T_3. The total

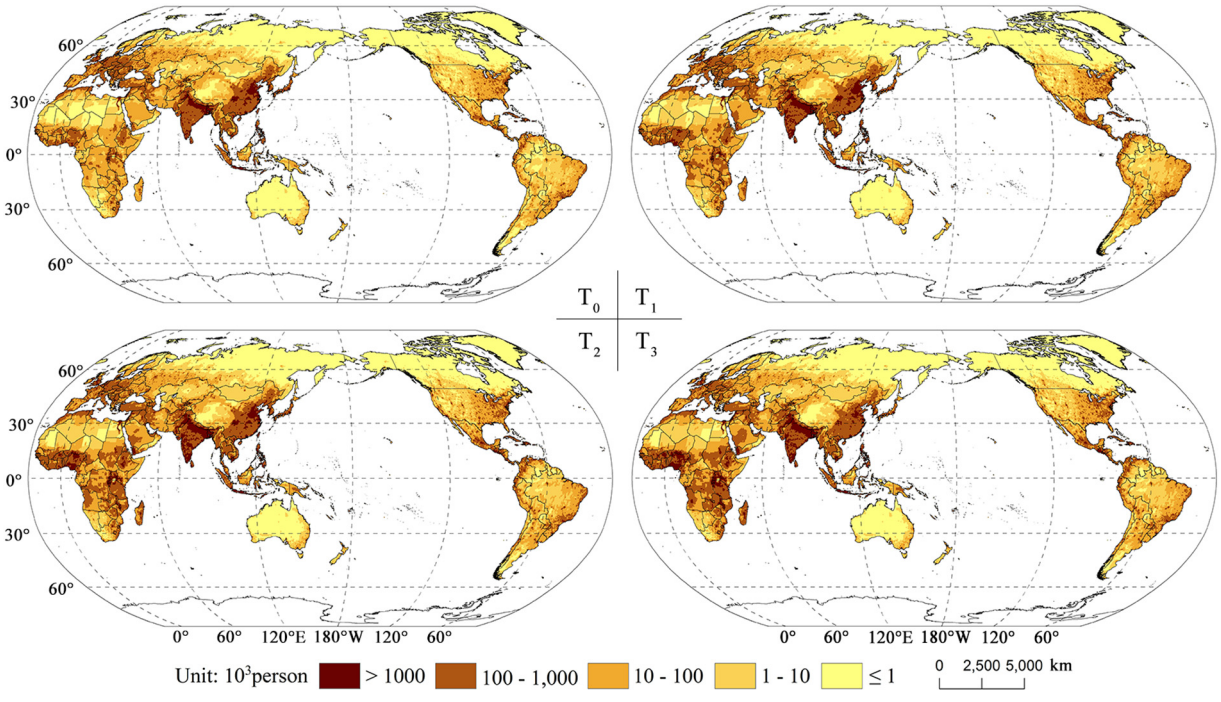

Fig. 2. Spatial distribution of the global population.

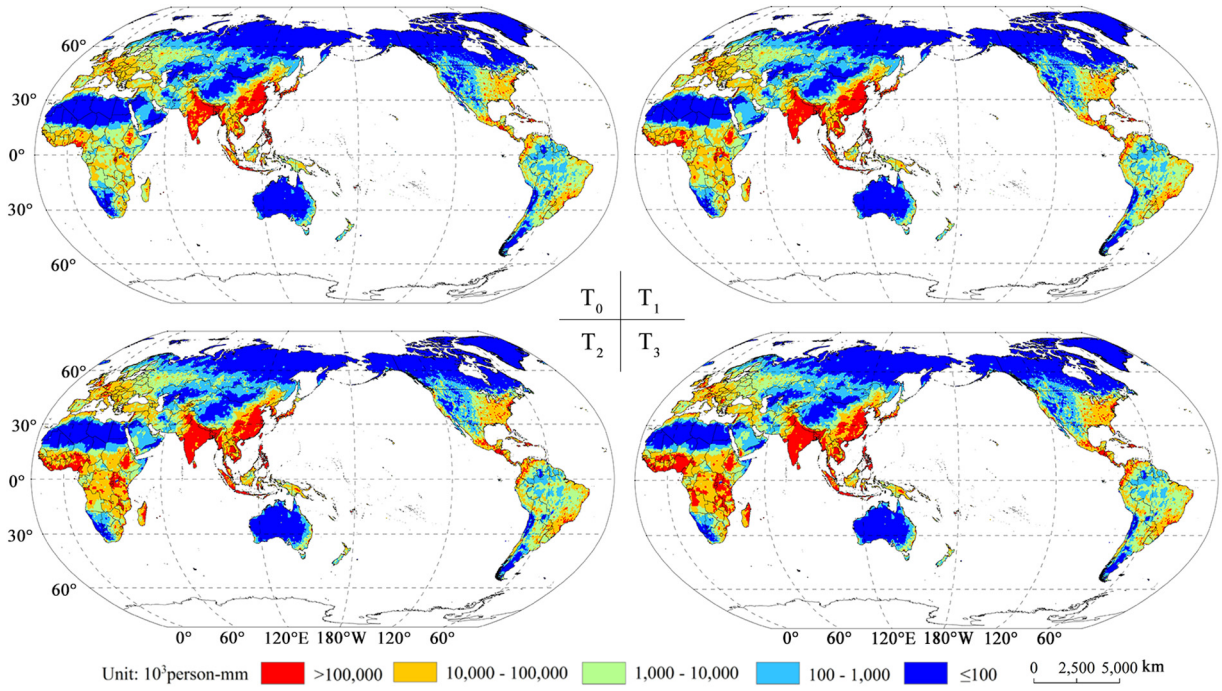

Fig. 3. Spatial distribution of the global population exposure to rainstorms.

exposure increases by $13.80 * 10^{11}$ person-mm, with a rate of 99%, from T_0 to T_3 (Table 3), and the total exposure in T_3 is almost twice that of T_0.

At the continental scale, Asia has the largest total exposure of approximately 3/5 of the global exposure, followed by Africa, and Oceania has the smallest total exposure. Asia and Europe show a trend of increasing first and then decreasing, but other continents have the same increasing trend as the global trend. Africa has the largest change rate of 485% from T_0 to T_3, while Europe has the smallest change rate of 0% (Table 3). It means that the total exposure of Africa in T_3 is about sixfold that of T_0, and there has been little change in the total exposure in Europe from T_0 to T_3.

The top 10 countries with the largest exposure for each period are shown in Fig. 4. China, India, Indonesia, Bangladesh, the United States, Brazil, Nigeria, and the Philippines always rank in the top eight countries for the four periods. The exposures of China and India are more than $2.50 * 10^{11}$ person-mm, which is three to nine times the exposures of the other six countries. In T_0, China has the largest exposure value, while India has the largest value for the other three periods. The change in total exposure for the top eight countries, with the exception of China, Bangladesh, and Brazil, shows the same trend as that of the world. Nigeria has the largest change rate of 577% from T_0 to T_3, but China shows a negative trend, with a change rate of −14% (Table 3).

Table 3
Total population exposure to rainstorms and the change rates.

	Total exposure (10^{11} person-mm)				*E_Rate* (%)			
	T_0	T_1	T_2	T_3	T_{1-0}	T_{2-1}	T_{3-2}	T_{3-0}
Global	13.91	20.53	25.06	27.71	48	22	11	99
*Asia	9.58	13.70	15.33	14.65	43	12	−4	53
**China	2.92	3.53	3.27	2.50	21	−7	−24	−14
**India	2.78	4.44	5.38	5.42	60	21	1	95
**Indonesia	0.79	1.12	1.24	1.25	42	11	1	59
**Bangladesh	0.68	1.10	1.34	1.28	61	22	−4	88
**Philippines	0.31	0.54	0.71	0.79	78	30	11	158
*North America	1.05	1.50	1.86	2.13	43	24	14	102
**United States	0.58	0.78	0.91	1.02	33	17	12	75
*Europe	0.93	0.99	0.96	0.93	6	−2	−3	0
*Africa	1.45	3.05	5.41	8.48	110	77	57	485
**Nigeria	0.31	0.66	1.25	2.09	114	88	68	577
*South America	0.85	1.22	1.41	1.43	44	16	1	69
**Brazil	0.47	0.65	0.70	0.67	38	9	−5	43
*Oceania	0.05	0.08	0.09	0.10	44	19	5	81

3.3. Contribution rates of factors on global, continental, and country scale exposure

3.3.1. Global scale

At the global scale, the total population exposure changes from $13.91 * 10^{11}$ person-mm in T_0 to $27.71 * 10^{11}$ person-mm in T_3, and the contribution rates of each factor vary from 1% to 86%. From the composition of the total exposure change, the contribution rate of the population change effect is the largest (mostly above 70%), even reaching 86% in T_{1-0}, while the contribution rate of the joint change effect is the lowest (mostly below 10%). For T_{1-0}, T_{2-1}, and T_{3-2}, the climate change effect shows a straight upward trend that even exceeds the population change effect in T_{3-2}, with a contribution rate of 76%. The population change effect and the joint change effect shows a downward trend (Fig. 5).

3.3.2. Continental scale

Fig. 6 shows the contribution rates of factors for each continent. The population change effect is the main cause for the change in exposure for most continents, followed by the climate change effect, and finally the joint change effect. For most continents, the population change effect decreases over time. In T_{3-0}, Europe has the largest climate change effect of 51%, Oceania has the largest population change effect of 90%, and Africa has the largest joint change effect of 13%. For T_{1-0}, T_{2-1}, and T_{3-2}, the climate change effect of Asia shows a trend of first increasing and then decreasing, and the climate change effect of Asia reached 44% in T_{2-1}; the climate change effect of North America, Africa, South America, and Oceania shows a linear upward trend, in particular, South America and Oceania increase the most and even exceeds the population change effect in T_{3-2}; the climate change effect of Europe shows a trend of first decreasing and then increasing, and compared

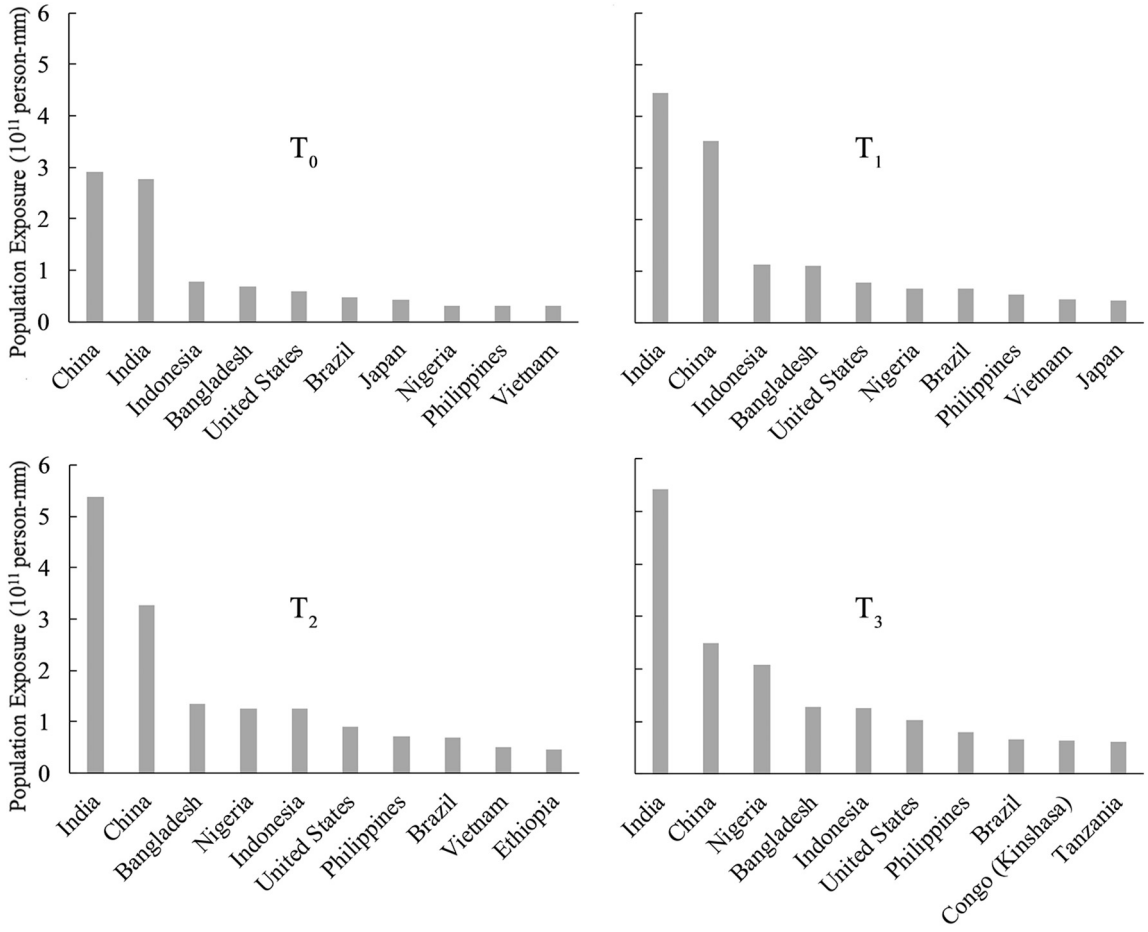

Fig. 4. Top 10 countries for the total population exposure to rainstorms.

to other continents, there is little difference between the climate change effect and the population change effect.

3.3.3. Country scale

To further examine the structure of exposure change, we decomposed each country's exposure change in different periods into climate change effect, population change effect, and joint change effect (Fig. 7 and Supplementary Table S2). In different time periods, for most countries the population change effect is the main contributor, in some countries it is the climate change effect, while the joint change effect has never been the main contributor. The contribution rate of the population change effect in some countries has reached approximately 100%. In T_{3-0}, there are 11 countries in which the climate change effect is greater than the population change effect. For T_{1-0}, T_{2-1}, and T_{3-2}, from the intersection of the climate change effect curve and the population change effect curve, it can be concluded that the number of countries whose climate change effect is larger than that of population change increases gradually, it is 4 in T_{1-0}, 17 in T_{2-1} and 50 in T_{3-2}; in addition, the maximum value of the climate change effect increases gradually, from 67% in T_{1-0} to 97% in T_{3-2}. The reason for the change of the contributor is that the population growth slows down while the rainfall from rainstorms grows faster with time.

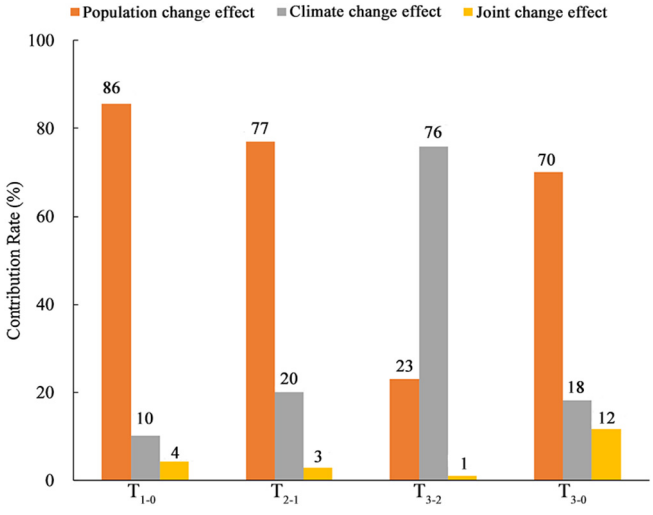

Fig. 5. Decomposition of the global change in population exposure.

Note: 1. Because of the relatively coarse spatial resolution of the result some countries are not included, and the total number of the countries we have analyzed is 173; 2. For T_{1-0}, T_{2-1}, T_{3-2}, and T_{3-0}, in order to express the differences between the three contributors more clearly, countries are sorted by the contribution rate of the climate change effect. So the same number on the horizontal axis represents different countries for the four periods.

3.3.4. The top eight countries

In order to analyze the drivers of exposure changes in various countries at different time periods in more details, we selected the top eight countries (in terms of population exposure) for further analysis—these

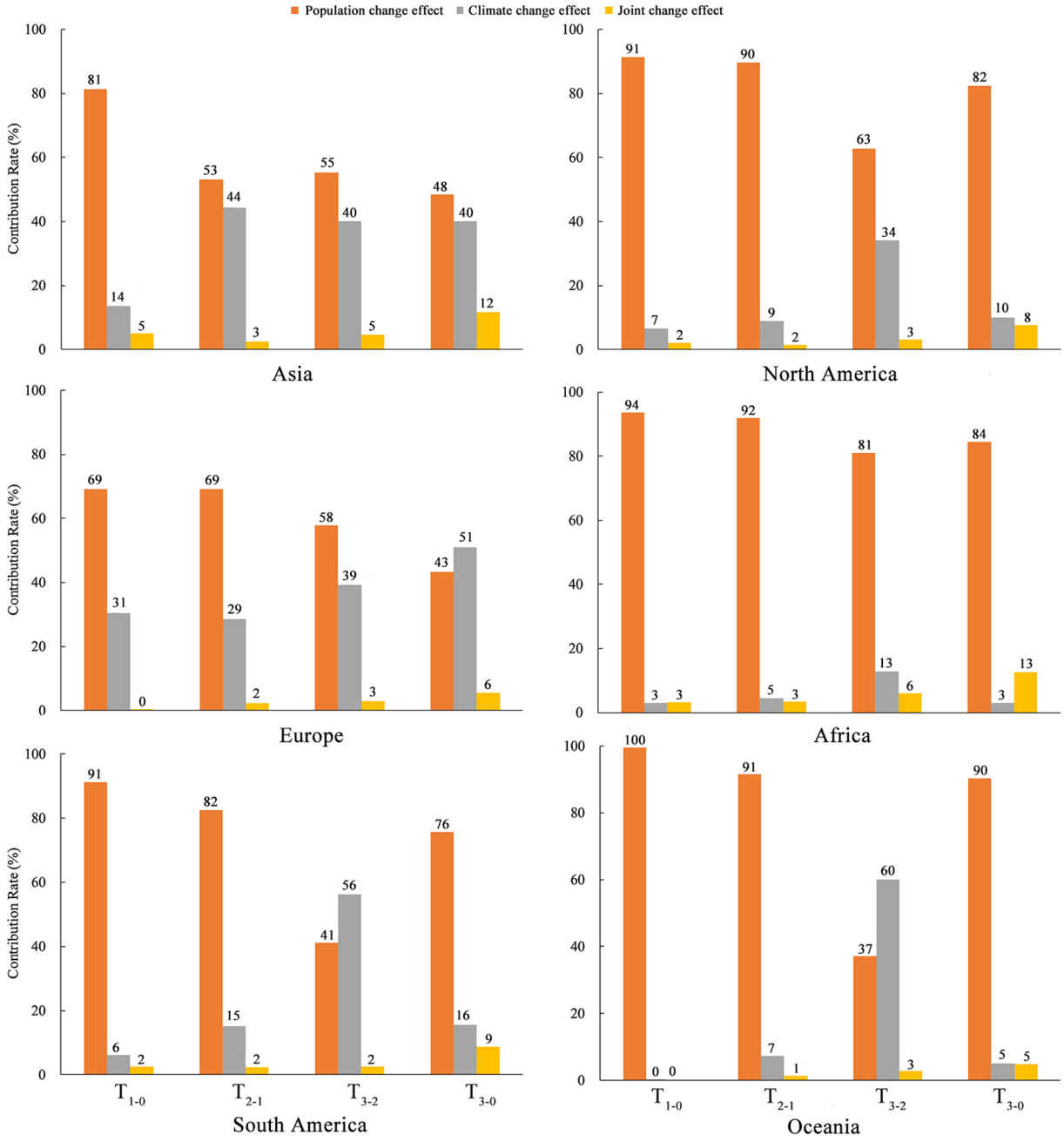

Fig. 6. Decomposition of the change in population exposure for each continent.

are China, India, Indonesia, Bangladesh, the United States, Brazil, Nigeria, and the Philippines. Fig. 8 shows that the population change effect is the main cause for the change in population exposure for the top eight countries. In T_{3-0}, the population change effect is dominant in all top eight countries, which all exceed 50%, and the climate change effect and the joint change effect always play a supporting role. For T_{1-0}, T_{2-1}, and T_{3-2}, the climate change effect of China shows a first increasing and then decreasing trend; that of Nigeria shows a first decreasing and then increasing trend; that of the other six countries shows an upward trend; and that of India, Indonesia, the United States, and the Philippines is dominant in T_{3-2}. Especially, the climate change effect in the Philippines has reached 74%. These top eight countries of population exposure always have heavy precipitation and/or large population, but their ranking by contribution rate of the climate change effect vary a lot, especially China and the Philippines. China's ranking is mostly about 140 in T_{1-0}, T_{2-1}, and T_{3-0}, but 59 in T_{3-2}; and that of the Philippines is 104 in T_{1-0}, 76 in T_{2-1}, 162 in T_{3-2}, and 93 in T_{3-0}.

4. Conclusions and discussion

The global population exposure to rainstorms was calculated for four periods, and the contribution rate of each contributor on population exposure change was quantitatively assessed in this study using data from global climate models and socioeconomic models (RCP4.5 and SSP2 scenario, respectively). The main conclusions are as follows:

(1) The population exposure to rainstorms shows a rapid increase from T_0 to T_1 and a slight increase from T_1 to T_3 in most regions. From T_0 to T_3, the total global population exposure to rainstorms increases by approximately 100%. Africa has the largest change rate of 485%, and Europe has the smallest change rate of 0%. Nigeria has the largest change

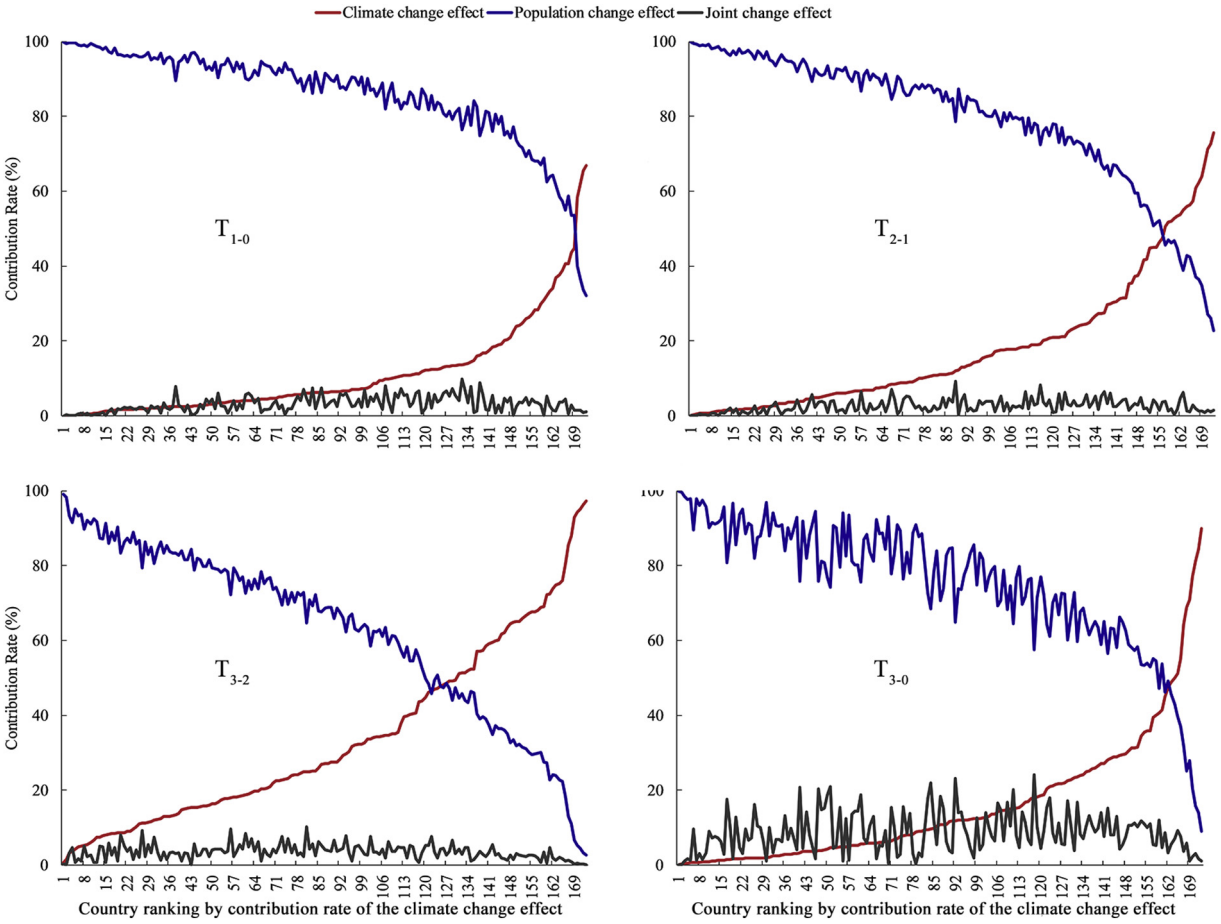

Fig. 7. Decomposition of the change in population exposure for each country.

rate of 577%, while China shows a negative trend with the change rate of −14%.

(2) The spatial distribution patterns of the global population exposure are similar for the four periods, and the areas with extremely high exposure and high exposure gradually increase from T_0 to T_3. The areas with extremely high exposure are mainly distributed in Asia (e.g., China, Japan, India, Bangladesh, the Philippines, and Indonesia), and scattered distributions are observed in Africa (e.g., Nigeria and Ethiopia). The countries with high total exposure have little volatility during the four periods, especially the top eight countries, which are always China, India, Indonesia, Bangladesh, the United States, Brazil, Nigeria, and Philippines.

(3) The exposure changes on global, continental, and country scales are mostly dominated by the population change effect, followed by the climate change effect, and finally the joint change effect. For different countries, the maximum value of the climate change effect is 97%, the population change effect is approximately 100%, and the joint change effect is 24%. From the composition of the total exposure change for each country, the number of countries whose climate change effect is larger than that of population change increases gradually, and reaches more than a quarter of the total in T_{3-2}. The reason for the change of the contributor is that the population growth slows down while the rainfall from rainstorms grows faster with time.

However, the precipitation and population data used in this study are model simulation results, they have some uncertainties. For the precipitation data, we have calculated the rainfall from rainstorms of each single model for the four periods, and we can see that the spatial patterns of rainfall in each period for the 21 downscaled CMIP5 GCMs are very similar, although some models have the results relatively high, such as the models of CCSM4, CESM1-BGC, and MRI-CGCM3 (Supplementary Fig. S1–4). Although many existing research results show that they are reliable, and we used the method of multi-model ensemble to reduce uncertainties, some uncertainties remain, especially for extreme values. Though the projected population data on global scale in SSPs scenarios is currently the best high-resolution and widely used one, it still has uncertainties. It is estimated under the assumption of the demographic transition occurs at average rates as societies develop without considering the change of each country's population policies, e.g., China's two-child policy. In future risk assessments, we need to verify and correct the simulation data to improve the accuracy of the results. On the other hand, climate change has led to an increase in rainstorms, but socioeconomic development is conducive to raising awareness for disaster prevention and increasing disaster management capabilities to reduce vulnerability. The population exposure to hazards depends not only on hazards but also on the regional fortification level; that is, the population in rainstorm-prone areas is not necessarily the exposed population. Therefore, it is necessary to consider the level of regional fortification in future research on population exposure to rainstorms.

Acknowledgements

This project was funded by the Ministry of Science and Technology of the People's Republic of China [grant number 2016YFA0602404, 2018YFC1508802]; Ministry of Education and State Administration of Foreign Experts Affairs, China [grant number B08008]. The NEX-GDDP

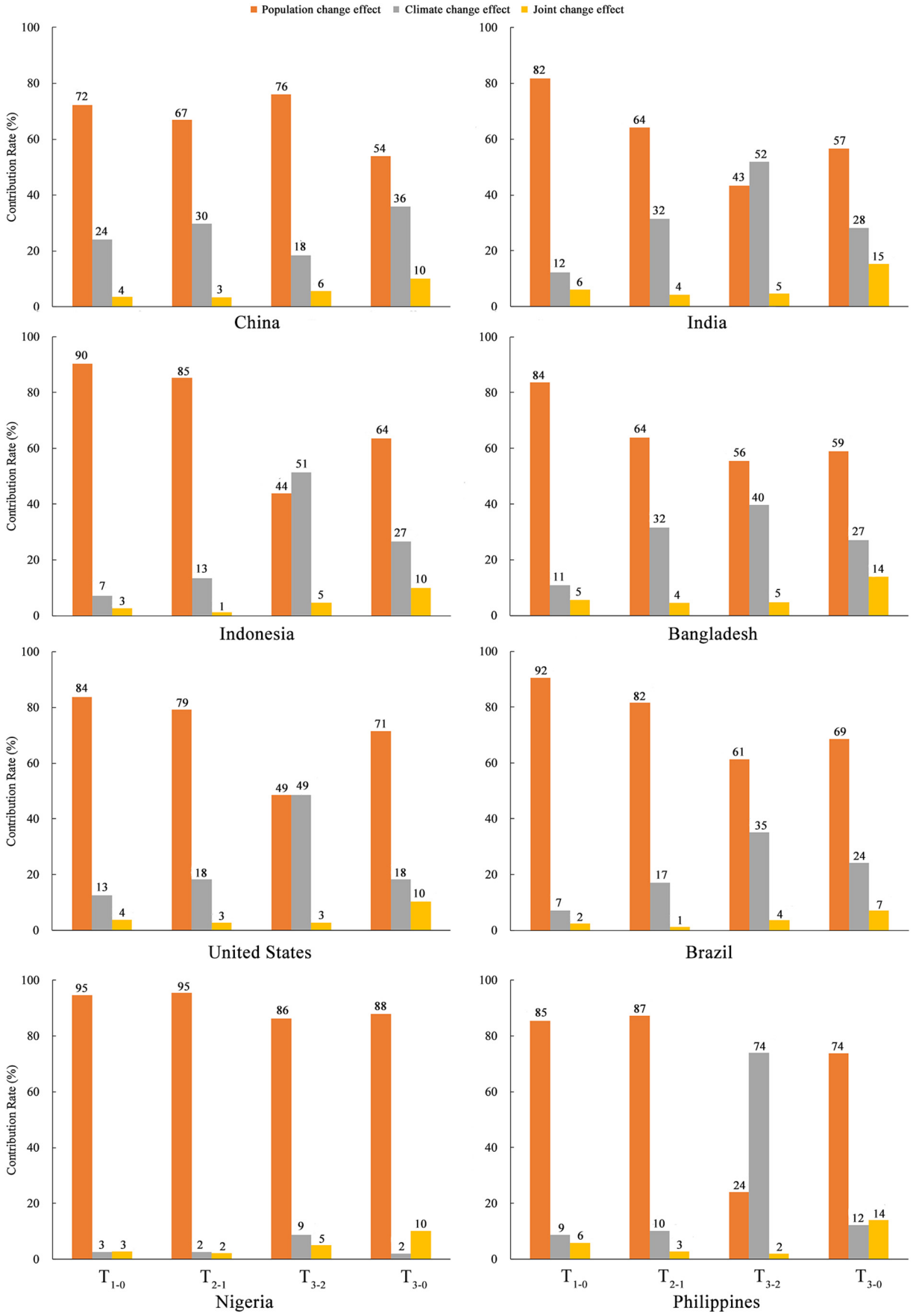

Fig. 8. Decomposition of the change in population exposure for the top eight countries.

dataset prepared by the Climate Analytics Group and NASA Ames Research Center and distributed by the NASA Center for Climate Simulation (NCCS), and the SSP2 data prepared by the Inter-Sectoral Impact Model Intercomparison Project (ISI–MIP), are used in this research and acknowledged. Special thanks to the two anonymous reviewers and editors for their critical comments, which helped to improve the quality of this paper significantly.

Appendix A. Supplementary information

Supplementary Table S1–2 and supplementary Fig. S1–4 of this article can be found online at https://doi.org/10.1016/j.scitotenv.2019.01.290.

References

Alexander, L.V., Zhang, X., Peterson, T.C., Caesar, J., Gleason, B., Klein Tank, A.M.G., Haylock, M., Collins, D., Trewin, B., Rahimzadeh, F., Tagipour, A., Rupa Kumar, K., Revadekar, J., Griffiths, G., Vincent, L., Stephenson, D.B., Burn, J., Aguilar, E., Brunet, M., Taylor, M., New, M., Zhai, P., Rusticucci, M., Vazquez-Aguirre, J.L., 2006. Global observed changes in daily climate extremes of temperature and precipitation. J. Geophys. Res. 111, D05109.

Barfus, K., Bernhofer, C., 2014. Assessment of GCM performances for the Arabian Peninsula, Brazil, and Ukraine and indications of regional climate change. Environ. Earth Sci. 72, 4689–4703.

Bonsal, B.R., Zhang, X., Vincent, L.A., Hogg, W.D., 2001. Characteristics of daily and extreme temperatures over Canada. J. Clim. 14, 1959–1976.

Chen, H., Sun, J., Li, H., 2017. Future changes in precipitation extremes over China using the NEX-GDDP high-resolution daily downscaled dataset. Atmos. Ocean. Sci. Lett. 10, 403–410.

Donat, M.G., Lowry, A.L., Alexander, L.V., O'Gorman, P.A., Maher, N., 2016. More extreme precipitation in the world's dry and wet regions. Nat. Clim. Chang. 6, 508–513.

Güneralp, B., Güneralp, İ., Liu, Y., 2015. Changing global patterns of urban exposure to flood and drought hazards. Glob. Environ. Chang. 31, 217–225.

Hanson, S., Nicholls, R., Ranger, N., Hallegatte, S., Corfee-Morlot, J., Herweijer, C., Chateau, J., 2011. A global ranking of port cities with high exposure to climate extremes. Clim. Chang. 104, 89–111.

IPCC, 2012. Summary for policymakers. In: Field, C.B., Barros, V., Stocker, T.F., Qin, D., Dokken, D.J., Ebi, K.L., Mastrandrea, M.D., Mach, K.J., Plattner, G.-K., Allen, S.K., Tignor, M., Midgley, P.M. (Eds.), Managing the Risks of Extreme Events and Disasters to Advance Climate Change Adaptation. A Special Report of Working Groups I and II of the Intergovernmental Panel on Climate Change. Cambridge University Press, Cambridge, UK, and New York, NY, USA (582 pp).

IPCC, 2014. In: Core Writing Team, Pachauri, R.K., Meyer, L.A. (Eds.), Climate Change 2014: Synthesis Report. Contribution of Working Groups I, II and III to the Fifth Assessment Report of the Intergovernmental Panel on Climate Change. IPCC, Geneva, Switzerland (151 pp).

Jones, B., O'neill, B.C., McDaniel, L., McGinnis, S., Mearns, L.O., Tebaldi, C., 2015. Future population exposure to US heat extremes. Nat. Clim. Chang. 5, 652–655.

Jongman, B., Ward, P.J., Aerts, J.C.J.H., 2012. Global exposure to river and coastal flooding: long term trends and changes. Glob. Environ. Chang. 22, 823–835.

Jongman, B., Winsemius, H.C., Aerts, J.C.J.H., Coughlan De Perez, E., Van Aalst, M.K., Kron, W., Ward, P.J., 2015. Declining vulnerability to river floods and the global benefits of adaptation. Proc. Natl. Acad. Sci. 112, E2271–E2280.

Liang, P., Xu, W., Ma, Y., Zhao, X., Qin, L., 2017. Increase of elderly population in the rainstorm hazard areas of China. Int. J. Environ. Res. Public Health 14, 936.

Liu, Z., Anderson, B., Yan, K., Dong, W., Liao, H., Shi, P., 2017. Global and regional changes in exposure to extreme heat and the relative contributions of climate and population change. Sci. Rep. 7, 43909.

Maurer, E.P., Hidalgo, H.G., 2008. Utility of daily vs. monthly large-scale climate data: an intercomparison of two statistical downscaling methods. Hydrol. Earth Syst. Sci. 12, 551–563.

Min, S.-K., Zhang, X., Zwiers, F.W., Hegerl, G.C., 2011. Human contribution to more-intense precipitation extremes. Nature 470, 378–381.

O'Neill, B.C., Kriegler, E., Ebi, K.L., Kemp-Benedict, E., Riahi, K., Rothman, D.S., van Ruijven, B.J., van Vuuren, D.P., Birkmann, J., Kok, K., Levy, M., Solecki, W., 2017. The roads ahead: narratives for shared socioeconomic pathways describing world futures in the 21st century. Glob. Environ. Chang. 42, 169–180.

Palmer, T.N., Doblas-reyes, F.J., Hagedorn, R., Weisheimer, A., 2005. Probabilistic prediction of climate using multi-model ensembles: from basics to applications. Philos. Trans. R. Soc. B 360, 1991–1998.

Popp, A., Calvin, K., Fujimori, S., Havlik, P., Humpenöder, F., Stehfest, E., Bodirsky, B.L., Dietrich, J.P., Doelmann, J.C., Gusti, M., Hasegawa, T., Kyle, P., Obersteiner, M., Tabeau, A., Takahashi, K., Valin, H., Waldhoff, S., Weindl, I., Wise, M., Kriegler, E., Lotze-Campen, H., Fricko, O., Riahi, K., van Vuuren, D.P., 2017. Land-use futures in the shared socio-economic pathways. Glob. Environ. Chang. 42, 331–345.

Qin, D., Zhang, J., Shan, C., 2015. China National Assessment Report on Risk Management and Adaptation of Climate Extremes and Disasters. Science Press, China.

Sahany, S., Mishra, S.K., Salunke, P., 2018. Historical simulations and climate change projections over India by NCAR CCSM4: CMIP5 vs. NEX-GDDP. Theor. Appl. Climatol. https://doi.org/10.1007/s00704-018-2455-z.

Samouly, A.A., Luong, C.N., Li, Z., Smith, S., Baetz, B., Ghaith, M., 2018. Performance of multi-model ensembles for the simulation of temperature variability over Ontario, Canada. Environ. Earth Sci. 77, 524.

Thrasher, B., Maurer, E.P., McKellar, C., Duffy, P.B., 2012. Technical note: bias correcting climate model simulated daily temperature extremes with quantile mapping. Hydrol. Earth Syst. Sci. 16, 3309–3314.

Toreti, A., Naveau, P., Zampieri, M., Schindler, A., Scoccimarro, E., Xoplaki, E., Dijkstra, H.A., Gualdi, S., Luterbacher, J., 2013. Projections of global changes in precipitation extremes from coupled model intercomparison project phase 5 models. Geophys. Res. Lett. 40, 4887–4892.

United Nations Office for Disaster Risk Reduction (UNISDR), 2017. Terminology. https://www.unisdr.org/we/inform/terminology#letter-e/ (accessed 15 February 2018).

Van Vuuren, D.P., Carter, T.R., 2013. Climate and socio-economic scenarios for climate change research and assessment: reconciling the new with the old. Clim. Chang. 122, 415–429.

Westra, S., Alexander, L.V., Zwiers, F.W., 2013. Global increasing trends in annual maximum daily precipitation. J. Clim. 26, 3904–3918.

Winsemius, H.C., Jongman, B., Veldkamp, T.I.E., Hallegatte, S., Bangalore, M., Ward, P.J., 2018. Disaster risk, climate change, and poverty: assessing the global exposure of poor people to floods and droughts. Environ. Dev. Econ. 23, 328–348.

Wood, A.W., Maurer, E.P., Kumar, A., Lettenmaier, D.P., 2002. Long-range experimental hydrologic forecasting for the eastern United States. J. Geophys. Res. 107, 4429.

Wood, A.W., Leung, L.R., Sridhar, V., Lettenmaier, D.P., 2004. Hydrologic implications of dynamical and statistical approaches to downscaling climate model outputs. Clim. Chang. 62 (1–3).

Zhang, W., Zhou, T., Zou, L., Zhang, L., Chen, X., 2018. Reduced exposure to extreme precipitation from 0.5 °C less warming in global land monsoon regions. Nat. Commun. 9, 3153.